OUKA
The University of Osaka
Institutional Knowledge Archive

Title	Transition from brittleness to ductility in cast titanium alloys high-oxygen through microstructural refinement
Author(s)	Kariya, Shota; Issariyapat, Ammarueda; Huang, Jeff et al.
Citation	Materials Science and Engineering: A. 2026, 974, p. 150775
Version Type	VoR
URL	https://hdl.handle.net/11094/106627
rights	This article is licensed under a Creative Commons Attribution 4.0 International License.
Note	

The University of Osaka Institutional Knowledge Archive : OUKA

https://ir.library.osaka-u.ac.jp/

The University of Osaka

Materials Science & Engineering A 974 (2026) 150775

Contents lists available at ScienceDirect

Materials Science & Engineering A

journal homepage: www.elsevier.com/locate/msea

Transition from brittleness to ductility in cast titanium alloys high-oxygen through microstructural refinement

Shota Kariya [a,*], Ammarueda Issariyapat [a], Jeff Huang [a], Junko Umeda [a], Biao Chen [b], Jianghua Shen [c], Katsuyoshi Kondoh [a,**]

[a] Joining and Welding Research Institute, The University of Osaka, 11-1 Mihogaoka, Ibaraki, Osaka, 67-0047, Japan
[b] State Key Laboratory of Solidification Processing, Northwestern Polytechnical University, Xi'an, Shaanxi, 710072, PR China
[c] School of Aeronautics, Northwestern Polytechnical University, Xi'an, Shaanxi, 710072, PR China

ARTICLE INFO

Keywords:
Titanium
Oxygen
Solid solution
Ductility
Grain size
Cast
Grain refinement

ABSTRACT

Previous studies on the ductility of Ti–O alloys have reported two contrasting behaviors—brittleness and high ductility—yet the critical factors required to achieve high ductility remain unclear. In this study, we investigated the effects of oxygen content and microstructure on the tensile properties of cast Ti–O alloys containing 0.21–0.96 wt% oxygen. The alloys were subjected to homogenization heat treatment followed by hot extrusion or hot rolling to evaluate the influence of oxygen segregation and grain refinement on their ductility. Homogenization eliminated oxygen segregation, leading to improved elongation in alloys with oxygen contents up to 0.59 wt%. Furthermore, thermomechanical processing refined the grain structure and introduced prismatic textures, enabling a remarkable recovery of ductility even in alloys with oxygen contents up to 0.96 wt%. Notably, the extruded alloy exhibited an elongation exceeding 25% at 0.82 wt% oxygen while achieving an ultimate tensile strength (UTS) above 1000 MPa. A systematic investigation of alloys with controlled oxygen content and grain size revealed that, for oxygen levels above 0.4 wt%, fine-grained microstructures exhibited high ductility, whereas ductility decreased once the grain size exceeded a critical threshold. This critical grain size decreased progressively with increasing oxygen content. Fractographic analysis showed that grain boundary cracking dominated in coarse-grained specimens, while fine grains effectively suppressed crack propagation. These findings quantitatively demonstrate that the ductility of Ti–O alloys is governed jointly by oxygen content and grain size and provide a material design strategy for the effective utilization of interstitial elements.

1. Introduction

Titanium is distinguished by its exceptional properties, including high specific strength, superior corrosion resistance owing to its dense oxide layer, and outstanding biocompatibility. Consequently, it is utilized across a wide range of sectors, such as medical devices [1–6] and transportation equipment [7,8]. As of 2024, only seven countries—China, Japan, Russia, Kazakhstan, Saudi Arabia, the United States, and India—were capable of producing titanium sponge, which is the primary material for titanium metal manufacturing. Among these, China, Japan, and Russia account for 90% of the global production. Similarly, vanadium, a critical alloying element in key alloys such as Ti-6Al-4V, has reserves and refining facilities concentrated in specific regions including Russia, China, and South Africa [9]. This specific concentration poses a significant risk to the stable supply of titanium alloys. Therefore, the increasing demand for titanium materials has necessitated the material design and the development of recycling technologies that mitigate resource supply risks [10,11].

One of the approaches involves the development of techniques for oxygen utilization. In the context of titanium materials employed in aircrafts, the buy-to-fly ratio, which compares the weight of the raw material to that of the finished product, has been reported to range from 15 to 20 to 1. This ratio indicates that more than 90% of the material has been wasted [12–14]. This is because, during the forging process of titanium, an oxygen-rich layer, known as the alpha-case, forms on the surface of the component [15–17]. The alpha-case is formed through oxygen diffusion from the atmosphere into titanium at elevated temperatures, resulting in a hardened oxygen-rich α-Ti layer with severely

* Corresponding author.
** Corresponding author.
E-mail addresses: kariya.shota.jwri@osaka-u.ac.jp (S. Kariya), kondoh.katsuyoshi.jwri@osaka-u.ac.jp (K. Kondoh).

https://doi.org/10.1016/j.msea.2026.150775
Received 26 February 2026; Received in revised form 3 June 2026; Accepted 13 July 2026
Available online 14 July 2026
0921-5093/© 2026 The Authors. Published by Elsevier B.V. This is an open access article under the CC BY license (http://creativecommons.org/licenses/by/4.0/).

degraded ductility. Consequently, large portions of the oxygen-contaminated surface region must be removed after processing to avoid deterioration in mechanical properties, thereby generating a substantial amount of high-oxygen titanium scrap. Therefore, to improve the efficient utilization and recycling of titanium resources, it is essential to establish alloy and process design strategies capable of effectively utilizing oxygen-containing titanium materials.

The recycling and effective reutilization of titanium scrap have become increasingly important because titanium production is concentrated in limited countries and titanium manufacturing processes generate a large amount of oxygen-contaminated scrap. In particular, oxygen-enriched titanium scrap generated through thermomechanical processing and α-case removal is expected to increase with the expanding demand for titanium products. Although several studies have reported that oxygen-contaminated titanium scrap can be deoxidized through calciothermic or rare-earth-assisted reduction processes [18, 19], these treatments generally require additional processing steps, specialized reaction control, and increased energy consumption, resulting in higher recycling costs. Therefore, from both economic and resource-utilization viewpoints, the direct utilization of oxygen-containing titanium materials without complete deoxidation has recently been considered to be an effective strategy for sustainable titanium recycling.

Oxygen functions as an α-stabilizing element that incorporates into titanium crystals as an interstitial solid solution, together with nitrogen and carbon, thereby resulting in an elevation of the β-transus temperature [20–23]. This α-stabilizing effect originates from the greater thermodynamic stability and higher solubility of oxygen in the hcp α-phase than in the bcc β-phase. Oxygen preferentially occupies octahedral interstitial sites in α-Ti, thereby lowering the free energy of the α-phase and stabilizing the α crystal structure. Simultaneously, the interstitial solid solution of oxygen causes expansion of the α-Ti crystal lattice, leading to remarkable solid-solution strengthening [20–22]. However, the oxygen content in titanium is stringently regulated, with maximum permitted levels of 0.40 wt% in commercially pure titanium (ASTM Gr. 4) and 0.20 wt% in the widely utilized Ti-6Al-4V alloy (ASTM Gr. 5) [24]. This limitation is based on the premise that oxygen contributes to the embrittlement of titanium [20,22].

According to the pioneering study by Jaffee et al., in 1950, a 0.5 wt% oxygen level results in approximately 20% elongation at fracture; however, when the oxygen content increases to 0.75 wt%, the elongation decreases to less than 5% [20]. These early studies established the widely accepted understanding that oxygen causes severe embrittlement in titanium through interstitial solid-solution strengthening. In addition, because oxygen is readily introduced into titanium during melting, casting, and thermomechanical processing, oxygen-enriched brittle layers such as the α-case are easily formed, which further limits the effective utilization and recycling of titanium resources. Therefore, establishing microstructural control strategies capable of maintaining ductility even at elevated oxygen concentrations has become an important metallurgical issue from both scientific and industrial viewpoints.

Nevertheless, recent investigations employing modern thermomechanical processing techniques have demonstrated that high ductility can be retained even in Ti–O alloys containing oxygen concentrations significantly higher than the conventional specification range [25–31]. An early example was reported in 2010 by Yoshimura et al., who developed Ti–O sintered extruded alloys containing 1.5–2 wt% TiO2 additions (equivalent to 0.80–0.98 wt% oxygen). The Ti–0.80 wt% O alloy exhibited a UTS of 1040 MPa and an elongation at fracture of 25.1%, whereas the Ti–0.98 wt% O alloy achieved a UTS of 1133 MPa with an elongation of 13.4%, demonstrating an excellent strength–ductility balance [25]. In addition, Morita et al. reported that a Ti–0.71 wt% O rolled alloy achieved a UTS of 805 MPa and an elongation at fracture of 23.9% [30]. More recent studies have also shown that thermomechanical processing routes, including extrusion, rolling, and microstructural refinement, can effectively suppress brittle fracture and improve ductility in high-oxygen titanium alloys [26–31]. These findings suggest that the tensile ductility of Ti–O alloys is governed not only by oxygen concentration but also strongly by microstructural factors such as grain refinement, crystallographic texture, and oxygen distribution.

Therefore, the oxygen concentration range investigated in this study (0.21–0.96 wt%) was selected to systematically examine the oxygen-content region where previous classical studies and recent thermomechanical processing studies reported significantly different ductility behaviors. In particular, while early studies reported severe embrittlement above approximately 0.75 wt% oxygen, recent studies demonstrated that high ductility can still be achieved even at oxygen concentrations approaching 1 wt% through appropriate microstructural control. Thus, this oxygen range was selected to clarify the microstructural factors governing the transition from brittleness to ductility in high-oxygen Ti–O alloys.

Optimizing the utilization of titanium resources, which are subject to supply challenges, requires recycling titanium scrap with high oxygen content. However, this recycling process can result in reduced ductility, necessitating a comprehensive understanding of the impact of microstructure on the ductility of Ti–O alloys. In this study, Ti–O alloys fabricated through casting were employed as initial materials, and the effects of microstructural changes, induced by processes such as heat treatment and plastic deformation, on their tensile properties, particularly ductility, were investigated. This approach enabled a thorough evaluation of the relationships among the solute oxygen content, microstructure, and tensile properties. The objective was to establish foundational knowledge for the effective utilization of solid-solution strengthening using oxygen. The findings demonstrated that the removal of solute oxygen segregation during phase transformation and grain refinement through plastic deformation significantly enhanced the ductility of the Ti–O alloys. Furthermore, the conditions necessary to achieve high ductility even with high oxygen content, which was previously considered to be a cause of brittleness, were identified. This study provides new guidelines for material design to address the issue of reduced ductility, thereby facilitating the efficient recycling of titanium scrap with high oxygen content. These findings establish a crucial technological basis for the future circulation of Ti resources.

2. Experimental

Ti–O alloys with oxygen contents of 0.21, 0.42, 0.59, 0.82, and 0.96 wt% were first fabricated using vacuum arc remelting (VAR) using commercially available titanium sponge supplied by Toho Titanium Co., Ltd. and are referred to as "as-cast." The specific compositions of the alloys are listed in Table 1. In the as-cast Ti–O alloys, oxygen segregation can occur in the two-phase coexistence region during solidification and phase transformation, potentially causing an uneven distribution of oxygen within the solid solution. To address this issue, heat treatment was performed at 800 °C for 24 h in a vacuum furnace, termed as "cast-HT." After homogenization heat treatment, furnace cooling was applied under vacuum conditions at an approximate cooling rate of 0.07 °C/min.

Subsequently, extrusion or rolling was employed to refine the grain size. For the extrusion process, cylindrical billets with an initial diameter

Table 1
Chemical compositions of the Ti–O alloys used in this study.

					[wt%]
	O	N	Fe	C	H
Ti–0.21 wt% O	0.21	<0.01	<0.01	<0.01	<0.01
Ti–0.42 wt% O	0.42	<0.01	0.01	<0.01	<0.01
Ti–0.59 wt% O	0.59	<0.01	0.01	<0.01	<0.01
Ti–0.82 wt% O	0.82	<0.01	0.04	<0.01	<0.01
Ti–0.96 wt% O	0.96	<0.01	0.04	<0.01	<0.01

of 42 mm and length of 30 mm after preheating for 300 s and extruded with an extrusion ratio of 36 (φ42 → 7 mm) at a ram speed of 3.0 mm/s. Ti–O extrudates preheated at the temperatures listed in Table 2, where the α+β two-phase coexistence region exists, and then extruded, are indicated as D-ex; those preheated at 1100 °C, where the β single-phase is present, and then extruded, are termed β-ex. Subsequently, D-ex underwent a heat treatment at 600 °C for 24 h, referred to as D-ex-HT. For the rolling process, after preheating at 550 °C for 120 s, the sample was repeatedly rolled until a 70% reduction was achieved. These rolled sheets were then subjected to heat treatment at 550 °C for 3 h to alleviate residual strain, followed by another heat treatment at 700–870 °C for 3 h in a vacuum environment to control the grain size.

To evaluate possible oxygen contamination during thermomechanical processing and heat treatment, oxygen concentrations after processing were measured using an ONH analyzer. The increase in oxygen concentration during processing was limited to a maximum of approximately 0.03 wt%. Considering the relatively small magnitude of this increase compared with the designed oxygen compositions of the alloys, its influence on the tensile properties, particularly ductility, was considered negligible.

The microstructure and crystal orientations of the Ti–O alloy were analyzed using scanning electron microscopy (SEM, JSM-6500F; JEOL Ltd.) in conjunction with an electron backscatter diffraction system (EBSD/Orientation Imaging Microscopy, OIM, DigiView IV Detector; TSL Solutions Co., Ltd.). EBSD data were analyzed using OIM Analysis software (TSL Solutions Co., Ltd.) for grain orientation and texture evaluation. EBSD measurements were performed under conditions appropriate for grain orientation and texture analysis of each specimen. The distribution of the solute elements was evaluated using an electron probe microanalyzer (EPMA, JXA-8530F; JEOL Ltd.). Two types of tensile specimens were prepared for each material to assess the mechanical properties. The as-cast and cast-HT specimens were plate-type with a gauge section width of 2 mm, thickness of 1 mm, and length of 10 mm. In contrast, the extruded and rolled specimens were rod-type with a diameter of 3 mm and gauge length of 10 mm. Prior to tensile testing, all gauge sections were finished by mechanical machining to a surface roughness of Ra 1.6 in order to minimize the influence of surface defects on tensile behavior. Tensile tests were performed at room temperature using a universal testing machine (Autograph AG-X 50 kN; Shimadzu Corporation) at a strain rate of 5×10^{-4}/s to determine the tensile strength, 0.2% proof stress, and elongation at fracture.

3. Results

3.1. Microstructure and tensile properties of Ti–O cast materials

Cast Ti–O alloys may undergo solute oxygen segregation during cooling. As illustrated by the phase diagram [23], the alloy transitions through a region where the liquid and solid (β phase) coexist during solidification, followed by a region where the α and β phases coexist during phase transformation. During these transitions, solute oxygen is distributed from the liquid to the solid phase and from the β phase to the α phase. Because oxygen exhibits higher thermodynamic stability and solubility in the α phase than in the β phase, oxygen partitioning preferentially occurs toward the α phase during cooling through the α/β coexistence region. This process may cause solute oxygen segregation at the boundaries of the previous β and α phase grains. To address this issue, a homogenization heat treatment was performed at 800 °C. For Ti–0.59 wt% O, the microstructural changes before and after heat treatment were examined using optical microscopy, with compositional images and oxygen distribution maps from SEM–EPMA analyses presented in Fig. 1.

Table 2
Summary of extrusion temperatures applied to the D-Ex samples.

	Extrusion temperature
Ti–0.21% O	890 °C
Ti–0.42% O	910 °C
Ti–0.59% O	930 °C
Ti–0.82% O	970 °C
Ti–0.96% O	1000 °C

The optical image of the as-cast material showed that it comprised prior β-Ti grains formed by the plate-like α-Ti grains. Analysis of the oxygen distribution within this structure, along with the compositional image, revealed two types of oxygen segregation. The first type occurred within plate-like grains, where the oxygen concentration is high at the grain centers and low near the boundaries. The second type was observed between the prior β-Ti grains, where the α-Ti grains within the prior β-Ti grains at the bottom of the observed field exhibited higher oxygen concentrations than those in the other prior β-Ti grains, particularly those in the upper part of the field of view. The first type of oxygen segregation within the plate-like grains is assumed to be because of the partitioning of oxygen from the β phase to the α phase. The O-rich centers and O-poor boundary areas of the α-Ti grains are presumed to correspond to the α and β phases, respectively, within the α/β coexistence region during the phase transformation. As the temperature decreases and the phase transformation from β to α progresses, plate-like α-Ti grains form within the β-Ti grains. At this stage, the partitioning of oxygen between the phases resulted in segregation within the plate-like grains. The second type of oxygen segregation between the prior β-Ti grains is attributed to the partitioning of oxygen from the liquid to the β phase. The O-rich prior β-Ti grains are believed to represent the primary β phase, and because of inadequate homogenization of oxygen during the subsequent cooling, the oxygen concentration in the α-Ti grains within these primary β phases became higher than that in their surroundings. These results indicate that oxygen segregation occurs through both liquid-to-solid partitioning during solidification and β-to-α partitioning during phase transformation, resulting in heterogeneous local oxygen concentrations in the as-cast Ti–O alloys.

Following homogenization heat treatment, a significant increase in grain size was observed. Prior to the heat treatment, the grains exhibited a plate-like morphology with widths measuring several tens of micrometers. However, after heat treatment, the grain size exceeded 1 mm, which is comparable to or even larger than that of the prior β-Ti grains. This indicates that grain growth occurred during homogenization heat treatment, resulting in the formation of large grains with low aspect ratios. Analysis of the oxygen distribution together with the compositional image revealed no detectable oxygen segregation either within the grains or at the grain boundaries, indicating that the two segregation modes observed in the as-cast condition were effectively eliminated.

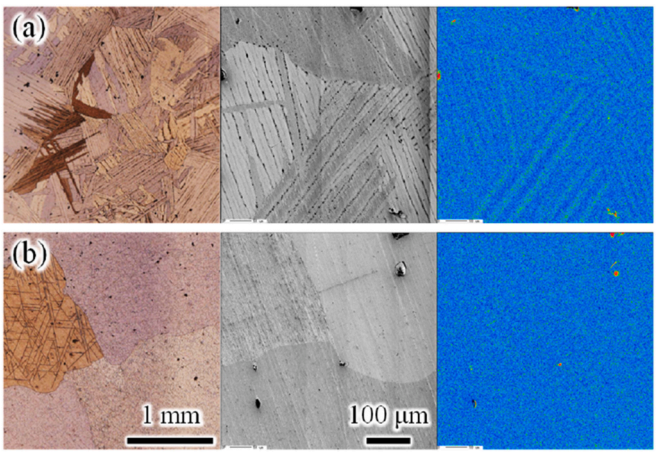


Fig. 1. Optical micrographs, SEM images, and EPMA oxygen distribution maps of (a) As-cast and (b) cast-HT of Ti-0.59 wt% O alloy.

Therefore, the homogenization heat treatment successfully reduced the local oxygen concentration gradients generated during solidification and phase transformation, resulting in a nearly uniform oxygen solid solution.

Subsequently, the influence of these microstructural modifications on the tensile properties was investigated. Figs. 2 and 3 illustrate the stress–strain curves and tensile properties, respectively. In the as-cast, with Ti–0.21, 0.42, and 0.59 wt% O, an increase in strength was observed with increasing oxygen content. However, at Ti–0.59 wt% O, the specimen fractured during the transition from the elastic to plastic phase without exhibiting any plastic deformation. For Ti–0.82 and 0.96 wt% O, a more pronounced brittle fracture behavior was observed; Ti–0.82 wt% O fractured within the elastic region at 458 MPa, whereas Ti–0.96 wt% O fractured at 328 MPa. The remarkable decrease in fracture stress at the highest oxygen concentrations suggests that the increase in local brittleness caused by excessive oxygen solid-solution strengthening exceeded the strengthening effect itself, thereby promoting premature crack initiation and unstable fracture before macroscopic plastic deformation could occur.

Conversely, in the cast-HT (b), where oxygen was homogenized, the strength also increased within the Ti–0.21–0.59 wt% O range as the oxygen content increased, similar to the as-cast. Regarding elongation at fracture, the as-cast Ti–0.42 wt% O and Ti–0.59 wt% O exhibited elongations of 8.1% and 1.1%, respectively, whereas in the cast-HT material, these values increased to 16.1% and 6.4%, respectively. For Ti–0.59 wt % O, clear plastic deformation was observed. In Ti–0.82 and 0.96 wt% O, fracture still occurred in the elastic region, similar to the as-cast material; the fracture stresses were 539 MPa for Ti–0.82 wt% O and 280 MPa for Ti-0.96 wt% O. The tensile ductility of cast Ti–O alloys is considered to be influenced by the competitive relationship among oxygen homogenization, coarse-grain-induced mechanical anisotropy, and oxygen embrittlement. Although the elongation of the Ti–0.21 wt% O alloy decreased after heat treatment, the Ti–0.42, 0.59, and 0.82 wt% O alloys exhibited improved ductility compared with the as-cast condition. The reduction in ductility observed in the Ti–0.21 wt% O alloy is considered to be associated with the development of coarse grains during heat treatment and the resulting enhancement of mechanical anisotropy. Because the grain size after homogenization became significantly larger than the cross-sectional dimensions of the tensile specimens (1 mm × 2 mm), the number of grains within the gauge section was limited. Under such conditions, the tensile response became highly sensitive to the crystallographic orientation distribution of the individual coarse grains contained within each specimen. Consequently, depending on the grain orientations in the gauge section, the mechanically anisotropic deformation behavior could deteriorate the apparent tensile ductility. In contrast, the improved ductility observed in the Ti–0.42–0.82 wt% O alloys suggests that oxygen homogenization may contribute to ductility recovery in cast Ti–O alloys.

Moreover, the Ti–0.42 and 0.59 wt% O cast-HT exhibited yield behavior, characterized by a reduction in the stress value during the transition from elastic to plastic deformation. This type of yield behavior has also been observed in titanium single crystals and rolled pure titanium with pronounced anisotropy [32–34]. In these heat-treated

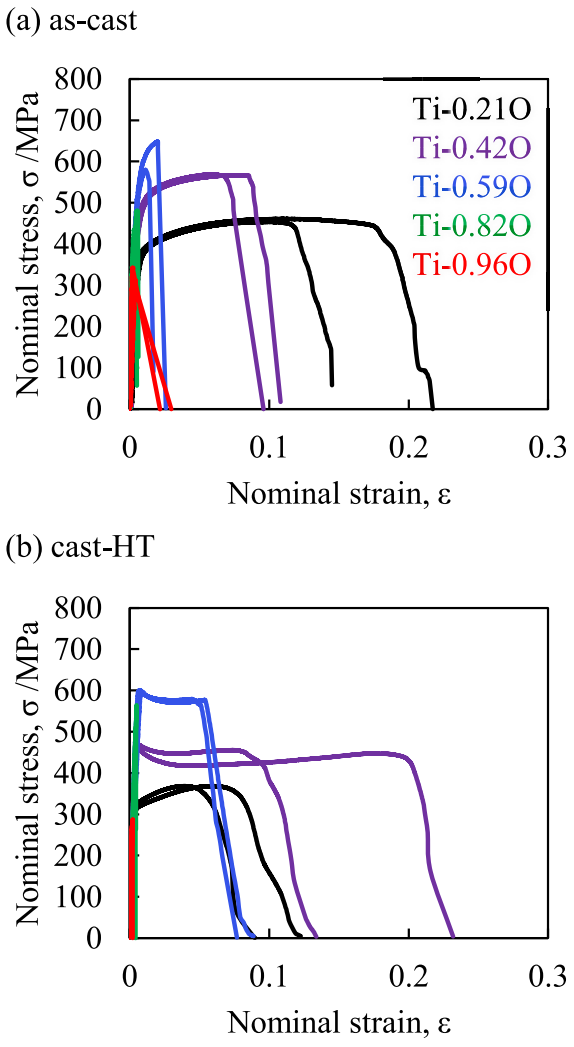


Fig. 2. The stress-strain curves of (a) as-cast and (b) cast-HT Ti-O alloys.

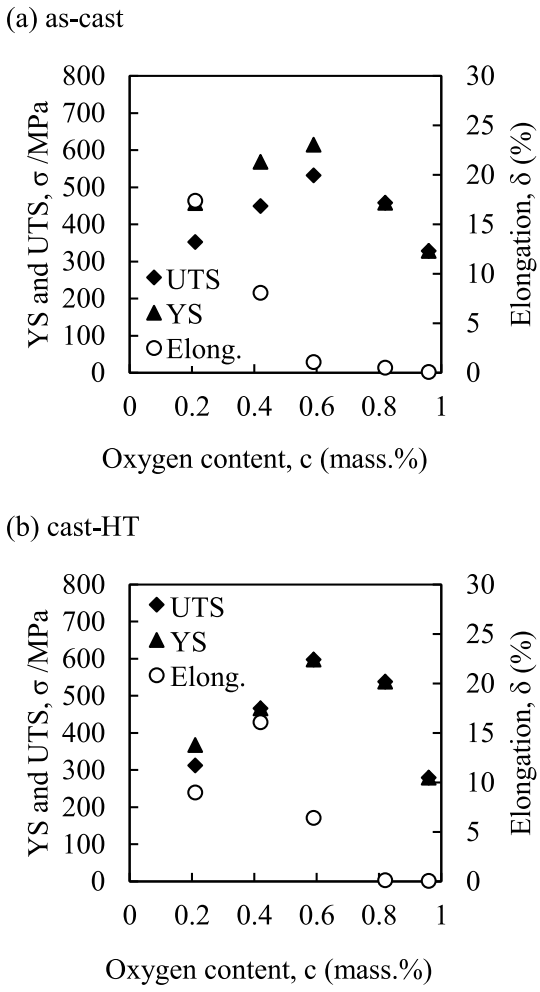


Fig. 3. The tensile properties of (a) as-cast and (b) cast-HT Ti-O alloys.

materials, the grain size was significantly larger than the cross-section of the specimen (1 mm × 2 mm), resulting in a limited number of grains in the tensile region. Consequently, the effect of anisotropy became more pronounced, which is presumed to have influenced the yield behavior. The yield behavior was particularly prominent in the Ti–0.42 and 0.59 wt% O alloys because these alloys retained sufficient deformability to initiate localized plastic deformation while simultaneously exhibiting strong crystallographic anisotropy associated with the coarse-grained microstructure. Under such conditions, plastic deformation preferentially initiated in grains with favorable orientations, resulting in discontinuous yielding and a temporary reduction in stress during the elastic-to-plastic transition. In contrast, in the higher-oxygen alloys, brittle fracture occurred before stable plastic flow could develop because of severe oxygen embrittlement, thereby suppressing the appearance of noticeable yield behavior.

3.2. Microstructure and tensile properties of cast and extruded Ti–O materials

In cast Ti–O alloys, the removal of segregated solute oxygen was observed to enhance the ductility when the oxygen solid solution content was maintained at 0.59 wt% or lower. However, when the oxygen content was increased to 0.82 wt% or higher, the elongation at fracture decreased to 0% in both the as-cast and cast-HT, with no subsequent improvement in ductility following heat treatment. Previous studies that reported highly ductile Ti–O alloys involved hot plastic work. Consequently, this study investigated whether hot extrusion processing could restore ductility in high-oxygen Ti–O alloys through grain refinement and texture formation.

The inverse pole figure (IPF) maps for β-Ex, D-Ex, and D-Ex-HT are illustrated in Fig. 4, the inverse pole figure in Fig. 5, and the grain size in Table 3. It has been observed that the shape and orientation of the grains formed during extrusion depend on the phase during processing.

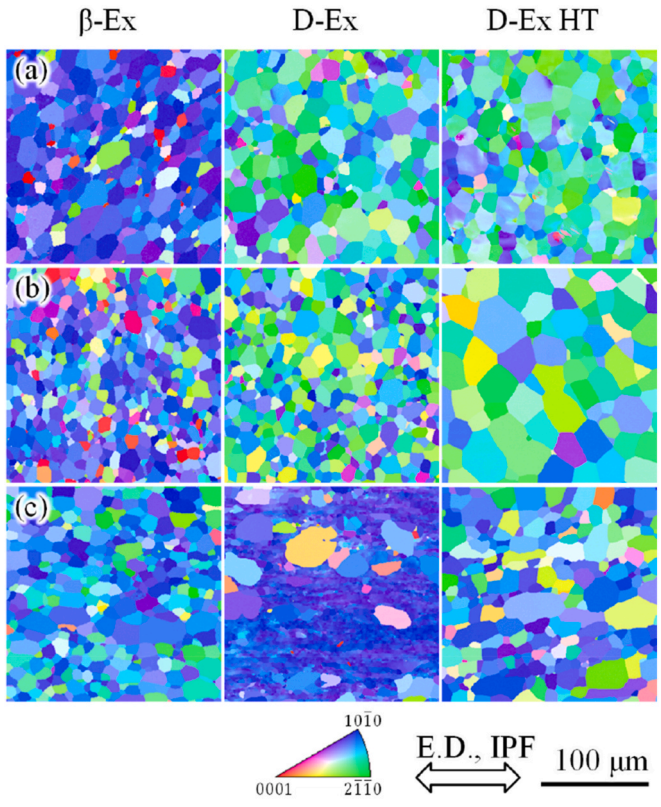


Fig. 4. IPF maps colored along the extrusion direction of B-Ex, D-Ex, and D-Ex HT for (a) Ti-0.21 wt% O, (b) Ti-0.59 wt% O, and (c) Ti-0.96 wt% O.

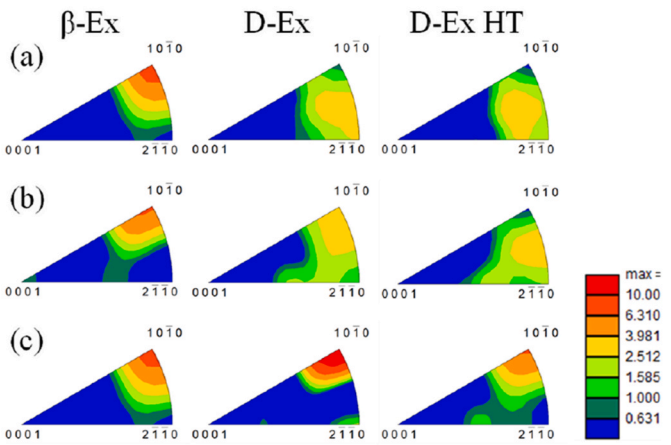


Fig. 5. Inverse pole figures along the extrusion direction of B-Ex, D-Ex, and D-Ex HT for (a) Ti-0.21 wt% O, (b) Ti-0.59 wt% O, and (c) Ti-0.96 wt% O.

Table 3
Grain size of Ti-O extrudate.

	β-EX	D-EX	[μm] D-EX HT
Ti–0.21O	15.4	17.4	19.2
Ti–0.42O	17.0	17.0	18.3
Ti–0.59O	12.5	12.9	30.3
Ti–0.82O	16.7	26.1	21.5
Ti–0.96O	14.9	38.8	19.2

Extrusion in the β phase results in deformed grains with a large aspect ratio owing to phase transformation post-processing, aligning their crystallographic orientation with the extrusion direction as (0001) and (101)//ED [35,36]. In contrast, extrusion in the α phase results in equiaxed grains with prismatic orientation along the extrusion direction (100) and (20)//E.D. [35,36]. All the extruded Ti–O alloys in this study exhibited a microstructure of equiaxed grains with prismatic orientation along the extrusion direction, indicating processing within the α phase. Although the billet preheating temperature for β-Ex was set at 1100 °C, the actual deformation temperature likely decreased because of heat loss during transfer and contact with the die maintained at 400 °C, resulting in partial transformation into the α+β two-phase region during extrusion. This explains why the microstructure and texture of β-Ex were similar to those of D-Ex.

The β-Ex exhibited an average grain size ranging from 12.5 to 17.0 μm. Similarly, the grain size of Ti-0.21–0.59 wt%O D-Ex was also between 12.9 and 17.4 μm. Additionally, D-Ex Ti–0.82 and 0.96 wt%O possessed large equiaxed grains measuring approximately 15–50 μm, together with larger grains that were elongated in the extrusion direction and characterized by low-angle grain boundaries of less than 5°. The formation of these elongated grains is considered to originate from heterogeneous deformation during extrusion caused by local differences in oxygen concentration inherited from the α+β two-phase state before extrusion. Regions with relatively low oxygen concentration underwent larger plastic deformation, resulting in deformation localization and formation of elongated grains with orientation gradients and low-angle grain boundaries. In addition, the elevated preheating temperatures required for high-oxygen alloys promoted grain growth prior to extrusion, which further contributed to the formation of coarse elongated grains. In D-Ex-HT, these smaller grains expanded, resulting in a more uniform grain size, averaging between 18 and 30 μm.

Table 4 lists the Schmid factors for the primary slip plane {100} of the materials under investigation. The Schmid factors of the extruded materials ranging from 0.44 to 0.46 for β-Ex, 0.41 to 0.45 for D-Ex, and 0.43 to 0.45 for D-Ex HT. The β-Ex Ti–0.21–0.96 wt% O, along with the

Table 4
Schmid factor of Ti-O extrudatein 1010 and 0001.

	B-Ex		D-Ex		D-Ex HT	
	{1010}	{0001}	{1010}	{0001}	{1010}	{0001}
Ti-0.21O	0.46	0.15	0.45	0.23	0.45	0.20
Ti-0.42O	0.45	0.11	0.41	0.27	0.43	0.23
Ti-0.59O	0.41	0.21	0.43	0.21	0.44	0.22
Ti-0.82O	0.46	0.10	0.42	0.22	0.43	0.20
Ti-0.96O	0.46	0.14	0.43	0.16	0.43	0.20

D-Ex and D-Ex HT Ti–0.82, 0.96 wt% O, demonstrated a (100) orientation. In contrast, the D-Ex and D-Ex HT Ti–0.21–0.59 wt% O exhibited a varied orientation from (100) to (20). However, no significant changes were observed in the Schmid factors.

EPMA analysis was performed to investigate the distribution of solute oxygen in β-Ex, D-Ex, and D-Ex HT. Fig. 6 illustrates the compositional image and oxygen distribution map for Ti–0.96 wt% O. In both β-Ex and D-Ex, regions with reduced solute oxygen levels were identified along the extrusion direction (indicated by the white arrow). Furthermore, in the D-Ex group, the oxygen content was uneven, with areas several tens of micrometers wide exhibiting a slight reduction in oxygen content (marked by the black arrow). This variation is attributed to the oxygen distribution between the α and β phases prior to extrusion. It is posited that β-phase grains, which contain less oxygen, were elongated during extrusion, resulting in areas with low oxygen content. Although the pre-extrusion heating temperature for β-Ex was 1100 °C, it decreased owing to the aforementioned reasons. During the two-phase state of the α and β phases, solute oxygen migration was incomplete, likely explaining why similar regions of reduced oxygen content were not observed in β-Ex. However, compared with the severe oxygen segregation observed in the as-cast materials, the degree of oxygen heterogeneity in the extruded materials was substantially reduced, indicating that plastic deformation during extrusion promoted partial homogenization of oxygen distribution. Subsequently, in D-Ex HT, which underwent heat treatment at 600 °C for 86.4 ks, the solute oxygen heterogeneity observed in D-Ex was eliminated. It is believed that this heat treatment effectively homogenized solute oxygen in the samples.

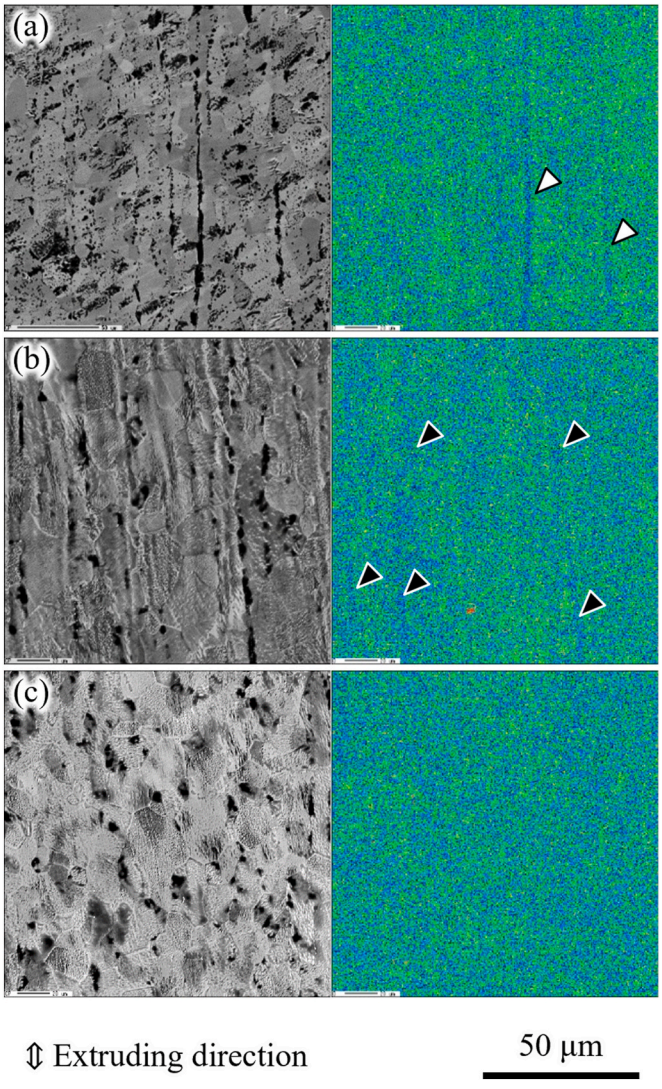


Fig. 6. EPMA analysis results of oxygen of (a) B-Ex and (b) D-Ex and (c) D-EX HT for Ti-0.96 wt% O extrudate.

In conclusion, hot extrusion processing resulted in grain refinement and the formation of a prismatic texture aligned with the extrusion direction. The grain size was substantially reduced from several millimeters prior to extrusion to several tens of micrometers after extrusion. During extrusion, oxygen segregation was observed owing to the distribution of oxygen between the α and β phases; however, this segregation was less pronounced than that observed during the casting process. These oxygen segregations were eliminated in D-Ex-HT following heat treatment.

The influence of these microstructural changes on the tensile properties and the stress–strain curves illustrated in Fig. 7 was investigated. For all β-Ex, D-Ex, and D-Ex HT, Ti–0.21–0.82 wt% O exhibited an elongation at fracture exceeding 20%. In the case of Ti–0.96 wt% O, β-Ex demonstrated significant variability; some specimens fractured after minimal local elongation, whereas others achieved approximately 5% elongation at fracture. This large scatter is considered to originate from the inherently unstable plastic deformation behavior at such high oxygen concentrations. Because Ti–0.96 wt% O was located near the critical oxygen concentration region where severe oxygen embrittlement occurred, small differences in local microstructure and deformation behavior likely caused significant variations in crack initiation and fracture behavior among the specimens. In contrast, D-Ex and D-Ex-HT exhibited reduced scatter, and the elongation at fracture exceeded 10%. However, in all cases, fracture occurred during uniform elongation and no distinct local necking was observed.

Consequently, a notable increase in strength was recorded for Ti–0.82 and 0.96 wt% O. Although Ti–0.82 and 0.96 wt% O experienced a reduction in strength owing to embrittlement in cast materials, the extruded materials exhibited excellent strength characteristics, 960–1015 MPa for Ti–0.82 wt% O and 1040–1045 MPa for Ti–0.96 wt% O, attributable to sufficient ductility. Consequently, for all the oxygen contents, both yield strength (YS) and UTS increased with increasing oxygen solid solution content because of solid solution strengthening [20–30].

A comparison of the tensile properties of D-Ex and D-Ex HT revealed no significant differences in the strength or ductility. This result indicates that the weak oxygen heterogeneity remaining after extrusion had only a limited influence on the macroscopic tensile properties. The dominant factor governing ductility recovery was therefore considered to be grain refinement introduced through extrusion rather than complete elimination of residual oxygen heterogeneity. In other words, although localized micro-yielding associated with oxygen heterogeneity may occur at the microscopic scale, its influence on the overall tensile response was much smaller than that of grain refinement.

Fig. 8 shows a comprehensive overview of the tensile properties. Extrusion enhanced the ductility for all the oxygen contents. Notably, even in Ti–0.21–0.42 wt% O, an improvement in ductility was observed; however, this enhancement was more pronounced in Ti–0.59–0.96 wt% O. Particularly, for Ti–0.59 wt% O, the ductility increased four-fold, and for Ti–0.82 and 0.96 wt% O, which initially exhibited 0% ductility in their cast form, it significantly increased to approximately 25% and

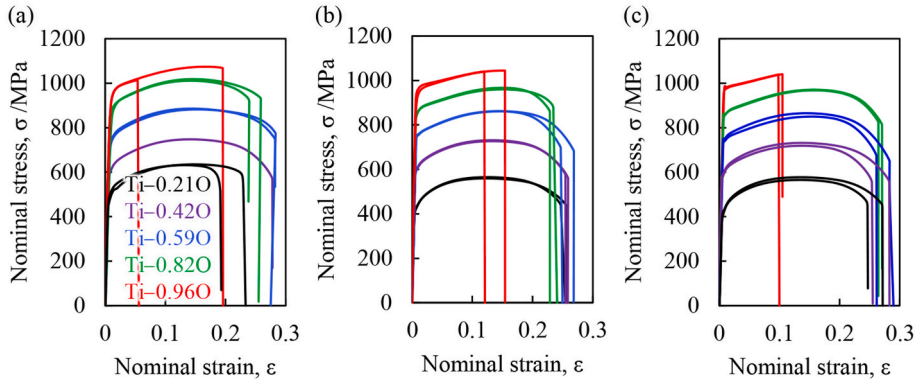


Fig. 7. The stress-strain curves of Ti-O extrudate of (a) B-Ex, (b) D-Ex, and (c) D-EX HT.

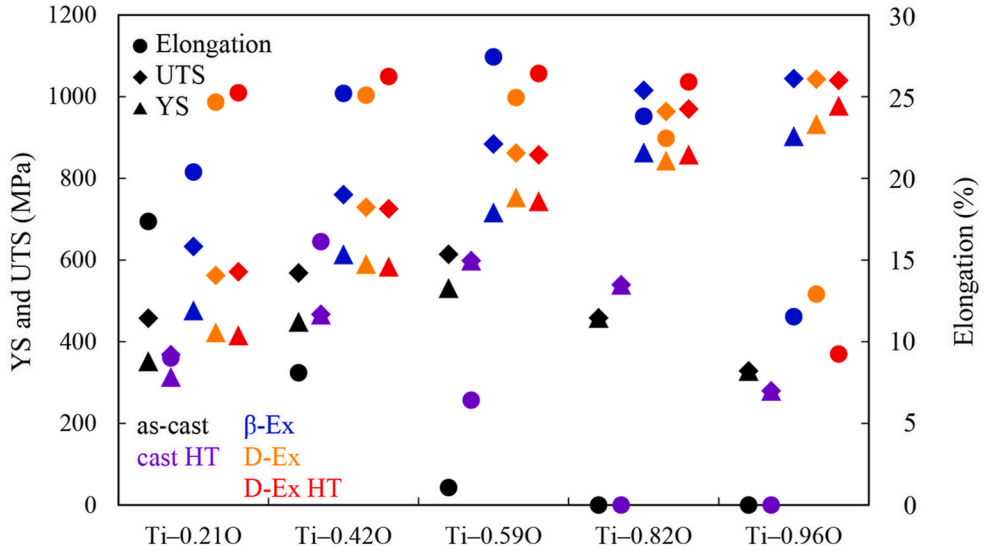


Fig. 8. The tensile properties of as-cast, cast HT, B-Ex, D-Ex, and D-EXHT.

10%, respectively. Both the UTS and YS exhibited an upward trend, with increases of approximately 100 MPa in Ti–0.21–0.42O and 250 MPa in Ti–0.59O. For Ti–0.82–0.96 wt% O, the as-cast materials fractured within the elastic region, resulting in low strength, whereas the extruded materials demonstrated adequate ductility, resulting in a notable increase in strength.

4. Discussion

In the cast materials, the incorporation of oxygen into a solid solution significantly diminishes the ductility. The maximum oxygen content permitting plastic deformation was determined to be 0.59 wt%. In contrast, following extrusion, the material demonstrated exceptional ductility, achieving an elongation at fracture of approximately 25%, even with an oxygen content as high as 0.82 wt%. Even in Ti–0.96 wt% O, a substantial level of ductility, with an elongation at fracture of

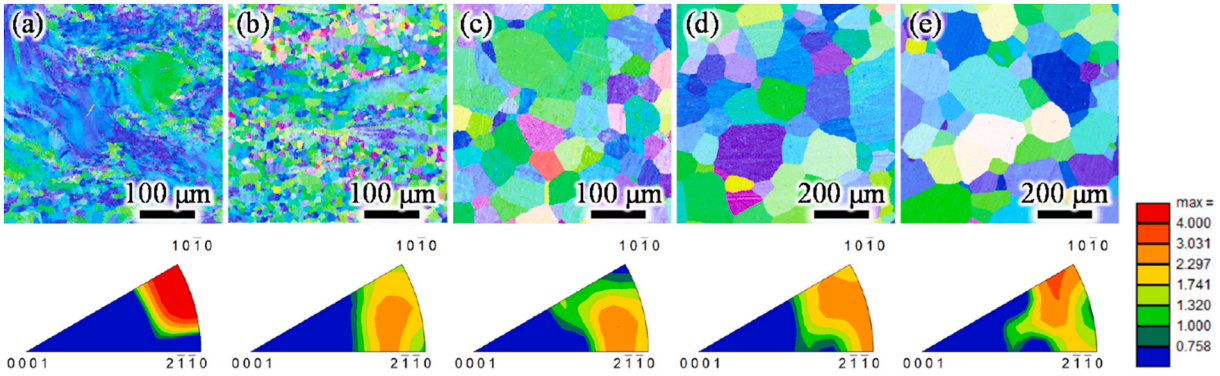


Fig. 9. IPF maps and corresponding inverse pole figures along the rolling direction of Ti-0.82 wt% O alloy for (a) as-rolled, (b) HT550, (c) HT700, (d) HT800, and (e) HT870.

approximately 10%, was observed. This enhancement was likely attributable to grain refinement. Therefore, this section examines the relationship between the ductility and grain size in Ti–O alloys and investigates their interconnections. Particularly, Ti–O alloys with controlled grain sizes were fabricated by rolling cast Ti–O alloys to develop a fine-grained structure, followed by heat treatment to alter the grain size. The tensile properties of these samples were assessed, and the correlation between the grain size and ductility was analyzed.

Fig. 9 illustrates the IPF maps and the inverse pole figure for the Ti–0.82 wt% O alloy in both its as-rolled and post-heat treatments, with the grain sizes specified in Table 5. Analysis of the as-rolled samples revealed that regardless of the oxygen content, all the samples exhibited a prismatic texture aligned with the rolling direction, similar to that observed in the extruded materials. This crystallographic orientation is a characteristic of rolled titanium alloys [36–39], where the basal planes align in the compression direction, resulting in a prismatic texture along the rolling direction. In the as-rolled sample, the grains were elongated in a direction perpendicular to the compression axis. Furthermore, significant orientation gradients within the grains indicate notable residual strain [40,41]. These orientation gradients qualitatively suggest the accumulation of geometrically necessary dislocations introduced during rolling deformation, although quantitative GND analysis was not performed in this study. The rolling process in this study was performed at 550 °C, which likely resulted in this microstructure because of insufficient dynamic recrystallization [42,43]. Furthermore, this temperature is within the single α-phase region, thereby avoiding the α+β phase region that could cause oxygen segregation, thereby ensuring a uniform distribution of dissolved oxygen.

In contrast, all the materials subjected to heat treatment exhibited equiaxed grains, and the orientation gradient was no longer evident. The grain size varied with the heat treatment temperature as follows: 14–48 μm at 550 °C, 59–81 μm at 700 °C, 116–220 μm at 800 °C, and 147–240 μm at 870 °C, indicating an increase in grain size with higher heat-treatment temperatures. This phenomenon is attributed to the recrystallization and grain growth during heat treatment. The grain size of Ti–0.42 wt% O closely aligns with the reported values for Ti–0.35 wt % O [44]. It was also observed that the grain sizes of Ti–0.79,0.96 wt% O were generally smaller than those of Ti–0.21, 0.42 wt% O, suggesting that the solute drag effect of O solute atoms inhibits grain growth [45–47]. Furthermore, the texture in the rolling direction remained prismatic across all the samples, with no significant changes in texture following grain growth.

The tensile properties of the as-rolled and post-heat treated materials were also assessed. Fig. 10 illustrates the dependence of the ultimate tensile strength (UTS) and elongation at fracture on the heat-treatment temperature. It was not feasible to determine the tensile properties of the as-rolled Ti–0.96 wt% O owing to cracking during the machining process. The UTS of the as-rolled materials for Ti–0.21 wt% O was recorded at 609 MPa, which increased to 934 MPa for Ti–0.59 wt% O and then further to 1037 MPa for Ti–0.82 wt% O. The elongation at fracture exceeded 20% for Ti–0.21 and 0.42 wt% O, whereas it was 10% for Ti–0.59 wt% O and decreased to 2% for Ti–0.82 wt% O. In contrast, following heat treatment at 550 °C, the UTS values were 506 MPa for Ti–0.21 wt% O, 808 MPa for Ti–0.59 wt% O, and 889 MPa for Ti–0.82 wt % O, indicating a reduction of more than 100 MPa compared with the as-rolled materials. This reduction is attributed to a reduction in the residual strain [48,49]. However, the elongation at fracture improved to 27% for Ti–0.59 wt% O and to 8% for Ti–0.82 wt% O. Ti–0.96 wt% O fractured within the elastic region, and its strength of 889 MPa was lower than that of Ti–0.82 wt% O.

Table 5
Grain size of hot rolled Ti–O alloys.

				[μm]
	HT550	HT700	HT800	HT870
Ti–0.21O	48.2	80.5	217.7	201.4
Ti–0.42O	16.3	76.3	180.9	240.2
Ti–0.59O	40.9	71.7	156.2	203.7
Ti–0.82O	24.7	58.6	137.9	146.7
Ti–0.96O	14.4	69.5	115.7	

Subsequent analyses examined the influence of heat-treatment temperature on the tensile properties. An increase in the heat-treatment temperature corresponded to a progressive decline in strength. Particularly, as the heat-treatment temperature increased from 550 to 870 °C, the strengths of the samples decreased as follows: Ti–0.21 wt% O, from 506 to 471 MPa; Ti–0.42 wt% O, from 682 to 624 MPa; Ti–0.59 wt% O, from 808 to 719 MPa; and Ti–0.82 wt% O, from 904 to 812 MPa. Conversely, the elongation at fracture for Ti–0.21 wt% O and Ti–0.42 wt% O remained consistently high, exceeding 25%, irrespective of the heat-treatment temperature. However, for Ti–0.59 wt% O, the elongation gradually decreased from 27% to 7%, and for Ti–0.82 wt% O, it declined from 8% to 1%. This reduction in elongation is attributed to an increase in the grain size.

We investigated the effects of oxygen content and grain size on elongation at fracture. Fig. 11 presents the relationship between the elongation at fracture, grain size, and oxygen content for the extruded and rolled materials examined in this study, along with data from previous studies [20,25,26,28–31]. For data lacking detailed reports on the grain size, representative values were used. For instance, the median was adopted for ranges; when only a single sample was presented, that value was applied to all the samples. When the oxygen content was up to 0.4 wt%, elongation at fracture exceeded 25% irrespective of the grain size. However, when the oxygen content exceeded 0.6 wt%, high ductility was observed in the fine-grain-size region, with a decrease in the ductility as the grain size increased. As the oxygen content increased, the grain size required for high ductility decreased. For Ti–0.59 wt% O, a grain size of 41 μm was required to achieve high ductility (20% elongation at fracture), whereas for Ti–0.82 wt% O, it was 24 μm. High ductility was also observed in the fine-grain-size region for Ti–0.96 wt% O; however, even at 15 μm grain size, the elongation at fracture was only approximately 10%. This relationship integrates the previous findings that characterized Ti–O alloys as brittle [20] with recent results indicating that Ti–O alloys can exhibit both high strength and ductility [25–31]. These results indicate that the ductility of Ti–O alloys is governed not only by oxygen concentration but also by the combined effects of oxygen concentration and grain size.

One possible explanation for the reduction in ductility with increasing grain size in Ti–O alloys is the presence of grain boundary cracks. Previous research demonstrated that in titanium alloys with an oxygen content exceeding 0.4 wt%, cracks form along the grain boundaries during tensile deformation [29,30]. Based on this observation, a hypothesis has been proposed regarding the relationship between grain size and ductility in Ti–O alloys [31] as the grain size becomes finer, the initial cracks at the grain boundary shorten, thereby reducing the stress concentration and preventing fracture because of cracks, ultimately enhancing the ductility of the material. Conversely, when the grain size was larger, the initial cracks became longer and the stress concentration at the crack tips resulted in crack propagation and premature fracture. This relationship is illustrated in Fig. 11. Similar beneficial effects of grain refinement on suppressing oxygen-related embrittlement have also been reported in titanium materials at low temperatures. Chong et al. [50] demonstrated that grain refinement effectively suppressed intergranular fracture and maintained tensile ductility in oxygen-containing titanium by reducing local stress concentration associated with oxygen embrittlement. Furthermore, our previous study on high-oxygen Ti alloys [51] reported that grain refinement effectively inhibited intergranular crack propagation during tensile deformation, resulting in a significant improvement in elongation. These findings support the present interpretation that grain refinement in Ti–O alloys suppresses grain boundary crack propagation and contributes to the transition from brittle to ductile behavior.

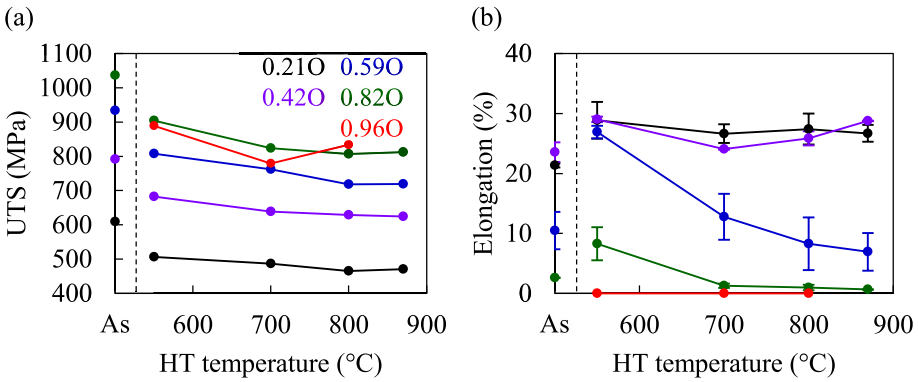


Fig. 10. The UTS and elongation at failure of hot rolled and heat-treated Ti-O alloys.

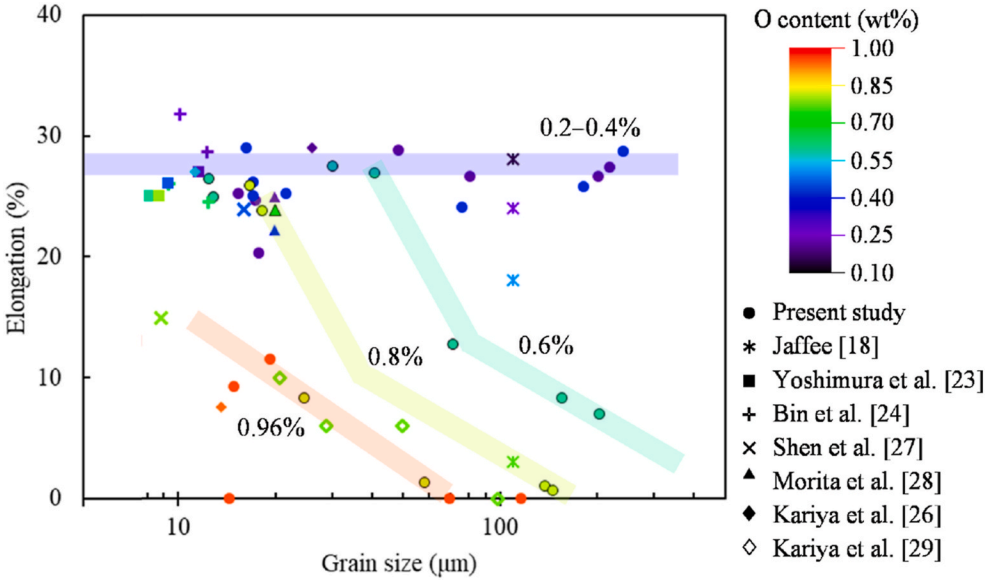


Fig. 11. Dependence of elongation to fracture on grain size for Ti-O alloys with various oxygen contents. The plotted data include present results from rolled and extruded samples, along with previously reported values from the literature [20,25,26,28–31].

Consequently, fracture surface analysis was performed to investigate the role of grain boundary cracks in the fracture of Ti–O alloys. Fig. 12 presents the results of the fracture surface analyses for Ti–0.21–0.81 wt % O specimens subjected to heat treatment at 550–800 °C. For Ti–0.21 wt% O, elongated dimples were visible across the entire fracture surface, and these dimples increased in size with larger grain sizes. In Ti–0.21 wt% O, no cracks were observed, regardless of the heat-treatment temperature. For Ti–0.42 wt% O, similar to Ti–0.21 wt% O, elongated dimples proportional to the grain size were observed throughout the fracture surface, with fine cracks appearing in some regions (white arrow). For Ti–0.59 and 0.82 wt% O, cracks were evident across the entire fracture surface (white arrow), with the maximum crack length reaching several hundred microns, indicating crack propagation. In specimens heat-treated at 550 °C, elongated dimples were observed across the entire surface. For those heat-treated at 700 and 800 °C, cleavage fracture surfaces were observed (black arrow), and their proportions increased with higher heat treatment temperatures. Furthermore, the fracture surfaces displayed a distinct granular appearance, indicating grain boundary fractures. These findings support the hypothesis that grain boundary cracks in Ti–O alloys influence their ductility. In fine-grained microstructures, the impact of grain boundary cracks on fracture is minimal, whereas in coarse-grained microstructures, grain boundary cracks cause grain boundary fracture and embrittlement.

5. Conclusion

A comprehensive examination of the oxygen segregation, grain size, and tensile properties, particularly ductility, of cast Ti–O alloys with varying oxygen contents was performed to optimize the utilization of titanium scrap with elevated oxygen content. The results demonstrate that by appropriately controlling the microstructure, high ductility can be maintained even at increased oxygen levels, resulting in the development of new material design guidelines for the practical application of high-oxygen Ti alloys. The principal findings of this study are summarized below.

- ☐ In the cast materials, a notable decrease in ductility was observed when the oxygen solid solution content exceeds 0.59 wt%, which was attributable to oxygen segregation during solidification and phase transformation. However, the ductility was restored in Ti–0.59 wt% O by homogenizing the solute oxygen through heat treatment performed below the phase-transformation temperature.
- ☐ Hot extrusion and rolling processes resulted in a microstructure characterized by a substantial reduction in grain size and the development of a prismatic texture. This microstructural refinement causes high ductility, with elongation at fracture exceeding 25%, even in Ti–0.82–0.96 wt% O alloys, in which the as-cast material is prone to brittle fracture.

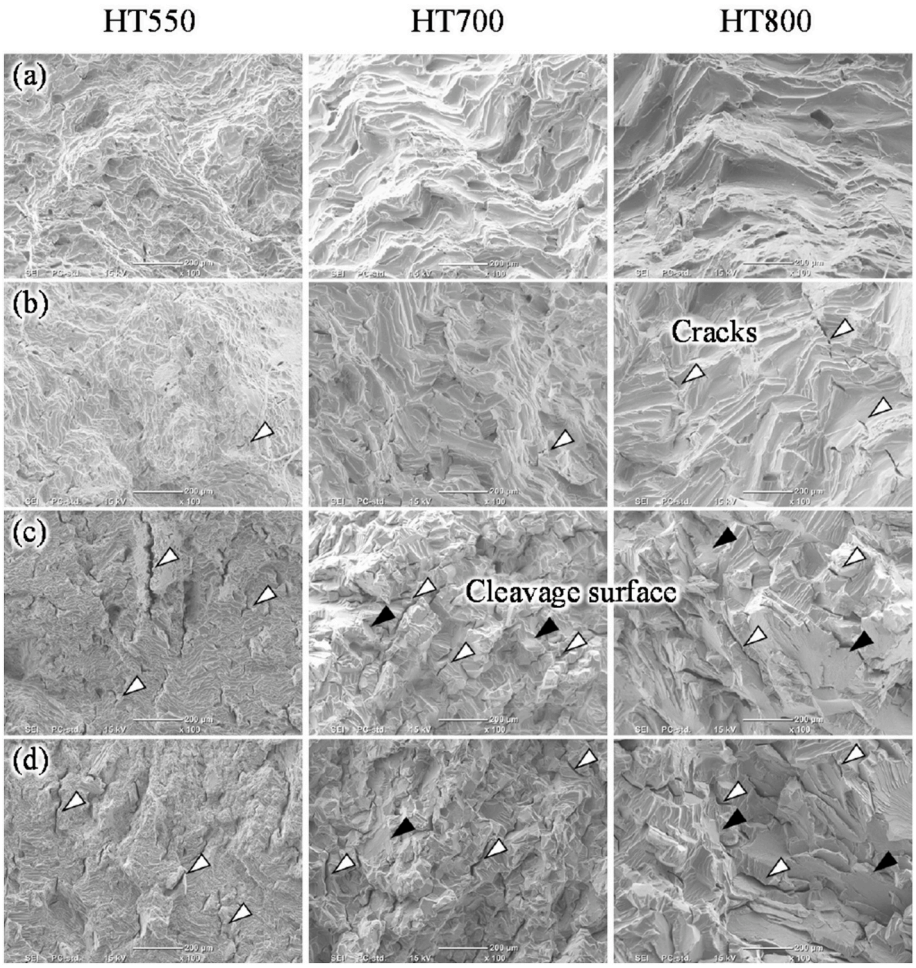


Fig. 12. Fractography images of Ti-O alloys: (a) Ti-0.21 wt% O, (b) Ti-0.42 wt% 0, (c) Ti-0.59 wt% O, and (d) Ti-0.82 wt% O after heat treated at 550 °C (HT550), 700 °C (HT700), and 800 °C (HT800). White arrow and black arrow indicate cracks and cleavage surface.

- Through a comprehensive analysis of the tensile properties of rolled materials with grain sizes regulated by heat treatment, this study quantitatively evaluated the effects of oxygen content and grain size on ductility. These findings indicate that when the oxygen content was 0.42 wt% or lower, high ductility was observed, irrespective of the grain size. Conversely, if the oxygen content exceeded this threshold, the ductility of the Ti–O alloys was significantly influenced by the grain size. Particularly, fine grains resulted in high ductility, whereas coarse grains resulted in brittleness. Furthermore, as the oxygen content increased, the grain size required to achieve high ductility decreased.
- Analysis of the fracture surface revealed that an increase in oxygen content was associated with more pronounced crack formation, whereas larger grain sizes contributed to more significant grain boundary fractures. These cracks were identified as grain boundary cracks, and it was demonstrated that the reduction in ductility of high-oxygen titanium alloys was attributable to these cracks. Conversely, grain refining effectively impeded the propagation of grain boundary cracks and the associated embrittlement, thereby elucidating the mechanism by which grain refinement enhances the ductility in Ti–O alloys.

These findings indicate that optimizing the utilization of titanium scrap with elevated oxygen levels necessitates achieving a uniform oxygen distribution, and critically, grain refining. These insights provide a valuable foundation for the sustainable use of Ti materials and process design strategies for high-strength, high-ductility Ti–O alloys.

CRediT authorship contribution statement

Shota Kariya: Data curation, Methodology, Visualization, Writing – original draft, Writing – review & editing. **Ammarueda Issariyapat:** Data curation, Writing – review & editing. **Jeff Huang:** Data curation, Writing – review & editing. **Junko Umeda:** Resources, Supervision, Validation. **Biao Chen:** Methodology, Validation. **Jianghua Shen:** Methodology, Validation. **Katsuyoshi Kondoh:** Conceptualization, Resources, Supervision, Validation, Writing – review & editing.

Declaration of competing interest

The authors declare that they have no known competing financial interests or personal relationships that could have appeared to influence the work reported in this paper.

Acknowledgements

We thank Toho Titanium Co., Ltd. for preparing the cast Ti–O alloy. This study was partially supported by the Inamori Foundation, Research Grant from the Japan Society for Technology of Plasticity, Environmental Restoration and Conservation Agency, and OU Master Plan Implementation Project promoted by The University of Osaka.

Data availability

Data will be made available on request.

References

[1] D. Banerjee, J.C. Williams, Perspectives on titanium science and technology, Acta Mater. 61 (2013) 844–879, https://doi.org/10.1016/j.actamat.2012.10.043.

[2] M. Geetha, A.K. Singh, R. Asokamani, A.K. Gogia, Ti based biomaterials, the ultimate choice for orthopaedic implants — a review, Prog. Mater. Sci. 54 (2009) 397–425, https://doi.org/10.1016/j.pmatsci.2008.06.004.

[3] K. Wang, The use of titanium for medical applications in the USA, Mater. Sci. Eng., A 213 (1996) 134–137, https://doi.org/10.1016/0921-5093(96)10243-4.

[4] M. Niinomi, M. Nakai, J. Hieda, Development of new metallic alloys for biomedical applications, Acta Biomater. 8 (2012) 3888–3903, https://doi.org/10.1016/j.actbio.2012.06.037.

[5] M.T. Mohammed, Development of a new metastable beta titanium alloy for biomedical applications, Karbala Int. J. Mod. Sci. 3 (2017) 224–230, https://doi.org/10.1016/j.kijoms.2017.08.005.

[6] M. Balazic, J. Kopac, M.J. Jackson, W. Ahmed, Review: titanium and titanium alloy applications in medicine, Int. J. Nano Biomaterials (IJNBM) 1 (2007) 3, https://doi.org/10.1504/IJNBM.2007.016517.

[7] S. Georgiadis, A.J. Gunnion, R.S. Thomson, B.K. Cartwright, Bird-strike simulation for certification of the Boeing 787 composite moveable trailing edge, Compos. Struct. 86 (2008) 258–268, https://doi.org/10.1016/j.compstruct.2008.03.025.

[8] Q. Zhao, Q. Sun, S. Xin, Y. Chen, C. Wu, H. Wang, J. Xu, M. Wan, W. Zeng, Y. Zhao, High-strength titanium alloys for aerospace engineering applications: a review on melting-forging process, Mater. Sci. Eng. A 845 (2022) 143260, https://doi.org/10.1016/j.msea.2022.143260.

[9] S.M. Jasinsk, Miner. Commod. Summ. 2025 (2025), https://doi.org/10.3133/mcs2025.

[10] E. Feng, D. Gao, Y. Wang, F. Yu, C. Wang, J. Wen, Y. Gao, G. Huang, S. Xu, Sustainable recovery of titanium from secondary resources: a review, J. Environ. Manag. 339 (2023) 117818, https://doi.org/10.1016/j.jenvman.2023.117818.

[11] O. Takeda, T. Ouchi, T.H. Okabe, Recent progress in titanium extraction and recycling, Metall. Mater. Trans. B Process Metall. Mater. Process. Sci. 51 (2020) 1315–1328, https://doi.org/10.1007/s11663-020-01898-6.

[12] J.C. Williams, R.R. Boyer, Opportunities and issues in the application of titanium alloys for aerospace components, Metals (Basel) 10 (2020) 705, https://doi.org/10.3390/met10060705.

[13] M. Gebler, A.J.M. Schoot Uiterkamp, C. Visser, A global sustainability perspective on 3D printing technologies, Energy Policy 74 (2014) 158–167, https://doi.org/10.1016/j.enpol.2014.08.033.

[14] B. Dutta, F.H. (Sam) Froes, The additive manufacturing (AM) of titanium alloys, in: Titanium Powder Metallurgy, Elsevier, 2015, pp. 447–468, https://doi.org/10.1016/B978-0-12-800054-0.00024-1.

[15] M. Whittaker, Titanium in the gas turbine engine, in: Ernesto Benini (Ed.), Advances in Gas Turbine Technology, InTech, 2011, pp. 315–336, https://doi.org/10.5772/21524.

[16] A. Caballero, J. Ding, Y. Bandari, S. Williams, Oxidation of Ti-6Al-4V during wire and arc additive manufacture oxidation of Ti-6Al-4V during wire and arc additive manufacture, 3D Print. Addit. Manuf. 6 (2018) 91–98, https://doi.org/10.1089/3dp.2017.0144.

[17] P. Ouyang, G. Mi, P. Li, L. He, J. Cao, X. Huang, Non-isothermal oxidation behavior and mechanism of a high temperature near-α Titanium Alloy, Materials (Basel) 11 (2018) 2141, https://doi.org/10.3390/ma11112141.

[18] T.H. Okabe, C. Zheng, Y. ki Taninouchi, Thermodynamic considerations of direct oxygen removal from titanium by utilizing the deoxidation capability of rare Earth metals, Metall. Mater. Trans. B Process Metall. Mater. Process. Sci. 49 (2018) 1056–1066, https://doi.org/10.1007/s11663-018-1172-4.

[19] O. Takeda, T.H. Okabe, Recycling of Ti, in: Extr. Metall. Titan., Elsevier, 2020, pp. 363–387, https://doi.org/10.1016/B978-0-12-817200-1.00016-8.

[20] R.I. Jaffee, H.R. Ogden, D.J. Maykuth, Alloys of titanium with carbon, oxygen, and nitrogen, Trans. AIME 188 (1950) 1261–1266, https://doi.org/10.1007/bf03399142.

[21] H.T. Clark, The lattice parameters of high purity alpha titanium; and the effects of oxygen and nitrogen on them, Metals Trans 185 (1949) 588–589, https://doi.org/10.1007/bf03398899.

[22] M. Yan, W. Xu, M.S. Dargusch, H.P. Tang, M. Brandt, M. Qian, Review of effect of oxygen on room temperature ductility of titanium and titanium alloys, Powder Metall. 57 (2014) 251–257, https://doi.org/10.1179/1743290114Y.0000000108.

[23] J.L. Murray, H.A. Wriedt, The O−Ti (Oxygen-Titanium) system, J. Phase Equil. 8 (1987) 148–165, https://doi.org/10.1007/BF02873201.

[24] ASTM B265-20a, Specification for Titanium and Titanium Alloy Strip, Sheet, and Plate, ASTM International, West Conshohocken, PA, 2020, https://doi.org/10.1520/B0265-20A.

[25] T. Yoshimura, T. Thotsaphon, H. Imai, K. kondoh, Microstructural and mechanical properties of Ti composite reinforced with TiO_2 additive particles, Trans. JWRI 38 (2009) 37–41, https://doi.org/10.18910/6987.

[26] B. Sun, S. Li, H. Imai, T. Mimoto, J. Umeda, K. Kondoh, Fabrication of high-strength Ti materials by in-process solid solution strengthening of oxygen via P/M methods, Mater. Sci. Eng. A 563 (2013) 95–100, https://doi.org/10.1016/j.msea.2012.11.058.

[27] B. Chen, J. Shen, X. Ye, J. Umeda, K. Kondoh, Advanced mechanical properties of powder metallurgy commercially pure titanium with a high oxygen concentration, J. Mater. Res. 32 (2017) 3769–3776, https://doi.org/10.1557/jmr.2017.338.

[28] S. Kariya, M. Fukuo, J. Umeda, K. Kondoh, Quantitative analysis on light elements solution strengthening in pure titanium sintered materials by labusch model using experimental data, Mater. Trans. 60 (2019) 263–268, https://doi.org/10.2320/matertrans.Y-M2018849.

[29] J. Shen, B. Chen, J. Umeda, J. Zhang, Y. Li, K. Kondoh, An in-situ study on deformation and cracking initiation in oxygen-doped commercial purity titanium, Mech. Mater. 148 (2020) 103519, https://doi.org/10.1016/j.mechmat.2020.103519.

[30] M. Morita, S. Suzuki, Y. Kato, W. Li, O. Umezawa, Tensile deformation of texture-controlled titanium with high oxygen content at room temperature, Mater. Sci. Eng. A 793 (2020) 139660, https://doi.org/10.1016/j.msea.2020.139660.

[31] S. Kariya, A. Issariyapat, A. Bahador, J. Umeda, J. Shen, K. Kondoh, Effect of grain size on the tensile ductility and fracture mechanism of Ti–O alloys, Mater. Sci. Eng. A 874 (2023) 145068, https://doi.org/10.1016/j.msea.2023.145068.

[32] A. Churchman, The yield phenomena, kink bands and geometric softening in titanium crystals, Acta Metall. 3 (1955) 22–29, https://doi.org/10.1016/0001-6160(55)90006-7.

[33] H. Conrad, Effect of interstitial solutes on the strength and ductility of titanium, Prog. Mater. Sci. 26 (1981) 123–403, https://doi.org/10.1016/0079-6425(81)90001-3.

[34] J. Umeda, T. Tanaka, T. Teramae, S. Kariya, J. Fujita, H. Nishikawa, Y. Shibutani, J. Shen, K. Kondoh, Microstructures analysis and quantitative strengthening evaluation of powder metallurgy Ti–Fe binary extruded alloys with (α+β)-dual-phase, Mater. Sci. Eng. A 803 (2021) 140708, https://doi.org/10.1016/j.msea.2020.140708.

[35] J. Wan, B. Chen, J. Shen, W. Shi, K. Kondoh, S. Li, J.S. Li, Developing dual-textured titanium (Ti) extrudates via utilizing the β transus in commercially pure Ti, Mater. Des. 215 (2022) 110459, https://doi.org/10.1016/j.matdes.2022.110459.

[36] W. Li, Z. Chen, J. Liu, S. Zhu, G. Sui, Q. Wang, Rolling texture and its effect on tensile property of a near-α titanium alloy Ti60 plate, J. Mater. Sci. Technol. 35 (2019) 790–798, https://doi.org/10.1016/j.jmst.2018.10.032.

[37] S.F. Frederick, G.A. Lenning, Producing basal textured Ti-6Al-4V sheet, Metall. Trans. B 6 (1975) 601–605, https://doi.org/10.1007/BF02913854.

[38] N.P. Gurao, S. Sethuraman, S. Suwas, Evolution of texture and microstructure in commercially pure titanium with change in strain path during rolling, Metall. Mater. Trans. A Phys. Metall. Mater. Sci. 44 (2013) 1497–1507, https://doi.org/10.1007/s11661-012-1484-y.

[39] M. Battaini, E.V. Pereloma, C.H.J. Davies, Orientation effect on mechanical properties of commercially pure titanium at room temperature, Metall. Mater. Trans. A Phys. Metall. Mater. Sci. 38 (2007) 276–285, https://doi.org/10.1007/s11661-006-9040-2.

[40] H.B. Zhang, B. Wang, Y.T. Zhang, Y. Li, J.L. He, Y.F. Zhang, Microstructure evolution and deformation mechanisms of β phase in TiBw/Ti60 composites studied by reconstructing grain during the hot deformation, J. Alloys Compd. 825 (2020) 153872, https://doi.org/10.1016/j.jallcom.2020.153872.

[41] K. Chen, D.J. Huang, H. Li, N. Jia, W. Chong, Avoiding abnormal grain growth when annealing selective laser melted pure titanium by promoting nucleation, Scr. Mater. 209 (2022) 114377, https://doi.org/10.1016/j.scriptamat.2021.114377.

[42] S. Mironov, S. Zherebtsov, S.L. Semiatin, The grain-refinement mechanism during heavy cold-rolling of commercial-purity titanium, J. Alloys Compd. 895 (2022) 162689, https://doi.org/10.1016/j.jallcom.2021.162689.

[43] Y.B. Chun, S.K. Hwang, Static recrystallization of warm-rolled pure Ti influenced by microstructural inhomogeneity, Acta Mater. 56 (2008) 369–379, https://doi.org/10.1016/j.actamat.2007.09.040.

[44] F.X. Gil, D. Rodríguez, J.A. Planell, Grain growth kinetics of pure titanium, Scripta Metall. Mater. 33 (1995) 1361–1366, https://doi.org/10.1016/0956-716X(95)00367-5.

[45] F.J. Gil, J.A. Picas, J.M. Manero, A. Forn, J.A. Planell, Effect of the addition of palladium on grain growth kinetics of pure titanium, J. Alloys Compd. 260 (1997) 147–152, https://doi.org/10.1016/S0925-8388(97)00135-7.

[46] D.M. Field, K.R. Limmer, B.C. Hornbuckle, On the grain growth kinetics of a low density steel, Metals (Basel). 9 (2019) 12–15, https://doi.org/10.3390/met9090997.

[47] K. Okazaki, K. Morinaka, H. Conrad, Grain growth kinetics in Ti–C alloys, Trans. Japan Inst. Met 14 (1973) 208–212, https://doi.org/10.2320/matertrans1960.14.208.

[48] P. Chen, S.C. Mao, Y. Liu, F. Wang, Y.F. Zhang, Z. Zhang, X.D. Han, In-situ EBSD study of the active slip systems and lattice rotation behavior of surface grains in aluminum alloy during tensile deformation, Mater. Sci. Eng. A 580 (2013) 114–124, https://doi.org/10.1016/j.msea.2013.05.046.

[49] D.H. Wei, W.J. Zhang, L.P. Zhang, H.Y. Huang, R.Y. Chen, Y.W. Wu, X.F. Ma, Z. H. Xiong, Crystal plasticity simulation of hot deformation texture of titanium alloy considering alpha-beta transformation, IOP Conf. Ser. Mater. Sci. Eng. 538 (2019) 012006, https://doi.org/10.1088/1757-899X/538/1/012006.

[50] Y. Chong, R. Gholizadeh, T. Tsuru, R. Zhang, K. Inoue, W. Gao, A. Godfrey, M. Mitsuhara, J.W. Morris, A.M. Minor, N. Tsuji, Grain refinement in titanium prevents low temperature oxygen embrittlement, Nat. Commun. 14 (2023) 1–11, https://doi.org/10.1038/s41467-023-36030-0.

[51] S. Kariya, A. Issariyapat, A. Bahador, J. Umeda, J. Shen, K. Kondoh, Ductility improvement of high-strength Ti–O material upon heteromicrostructure formation, Mater. Sci. Eng. A 842 (2022) 143041, https://doi.org/10.1016/j.msea.2022.143041.